Cage Structure and Long-Range Order in Solid Rare Gas Matrixes: A Combined FTIR and XRD Study†

Erich Knözinger,* Ewald Babka, and Doris Hallamasek

Institut für Physikalische und Theoretische Chemie, Technische Universität Wien Veterinärplatz 1, Trakt GA, A-1210 Wien, Austria

Received: May 29, 2001

Infrared spectroscopy (FTIR) and X-ray diffractrometry (XRD) were applied in order to characterize solid rare gas matrixes containing SF_6 or CH_4 species as impurities. The two techniques may be considered as complementary insofar as FTIR probes the dynamics of the dopant species, which is more or less strongly influenced by the matrix environment, whereas XRD aims at the long-range order of the rare gas matrix, which is likely to depend on the type and amount of the dopant. In fact, the distortions induced in Ar matrixes by embedding perfectly isolated CH_4 and SF_6 monomer molecules are not seen by XRD since the respective contribution to the broadening of Bragg reflections is buried under the dominating contribution related to the crystallite size effect (Scherrer formula). The nonequilibrium conditions of the deposition process give rise to a mean crystallite diameter of less than 50 nm. From the trends observed for both position and width of the respective IR test bands in Ne, Ar, and Kr, it is concluded that the matrix cages for the CH_4 monomer are single substitutional sites, whereas for the SF_6 monomer the space required comprises that of six rare gas atoms in an octahedral arrangement. However, a tetrahedral cage consisting of four rare gas atoms may not be excluded definitely. The crystalline order of Ar is retained even at CH_4 concentrations that are undoubtedly related to the previously reported miscibility gap and to significant dimer formation detected by FTIR. On the other hand SF_6 dimer formation, again identified by FTIR, gives rise to a complete loss of coherent X-ray scattering of Ar and to the appearance of diffuse intensity in the XRD pattern attributed to an essentially amorphous Ar phase. The local Ar environment of an isolated monomer and of the monomer unit of an isolated dimer appear to be fundamentally different in the case of SF_6 and resemble each other for CH_4 as impurity. Obviously, the SF_6 dimer formation in Ar immediately heralds in an efficient phase separation process already at 1 mol % SF_6 even under the nonequilibrium conditions of matrix deposition. Under these conditions the phase separation in CH_4/Ar mixtures appears to be strongly kinetically hindered.

Introduction

In a simplistic view matrix isolation spectroscopy appears as a technique that makes gas phase spectra at extremely low-temperature available. On closer inspection this image has to be corrected according to the fact that even neon, the best classical solid matrix, is far from being ideal, i.e., from being noninteracting with the dopant. And, in addition, the closer a matrix material comes to ideality, the more difficult it is to guarantee perfect isolation of the real monomer species to be suspended in it. For thermodynamical reasons, the respective mixture always tends to cluster formation as the initial step of phase separation.[1]

As a matter of fact, there are only a few matrix relevant solid binary systems with phase diagrams exhibiting significant miscibility. Examples are CH_4/Ar[2,3] and CH_4/Kr.[4] For these exceptions of thermodynamically stable mixtures, the disordered matrix emerging from the process of gas phase deposition may be exposed to a thermally induced relaxation, i.e., to annealing without a major risk of phase separation. In most of the cryogenic matrix samples the thermodynamic equilibrium state is the phase separated system and, therefore, the perfect isolation of species is preferentially obtained in the nonrelaxed, disordered solid matrix frozen out during a fast process of gas phase deposition.

Only recently have nonclassical or quantum matrixes turned out to be particularly well suited for high-resolution studies aiming at a minimum influence of host−guest interaction. Both solid parahydrogen matrixes[5,6] and liquid helium droplets[7−9] were applied. The experimental setup required for these studies is certainly far from being the standard equipment of a matrix laboratory. This means that the great majority of matrix studies is and will be carried out in classical matrixes with the above-mentioned drawbacks and imperfections.

In the present study an attempt was made to correlate IR data that reflect the influence of the cage structure on the intramolecular dynamics of an isolated species and XRD data related to the respective long-range order of the matrix. In the interpretation procedure particular attention has to be paid to the discrimination of two different types of matrix disorder: (a) the equilibrium or equilibrium-like disorder attributed to dopant-induced distortions of a thermally relaxed matrix and (b) the disorder of a thermally nonrelaxed matrix that originates from a fast deposition process.

Experimental Section

Samples. The solid cryogenic samples were prepared by gas phase deposition. After thermal effusive expansion, the gaseous

† This paper is dedicated to Professor Hans Jörg Schnöckel (Universität Karlsruhe, Germany) on the occasion of his 60th birthday.

10.1021/jp012023l CCC: $20.00
Published on Web 08/11/2001

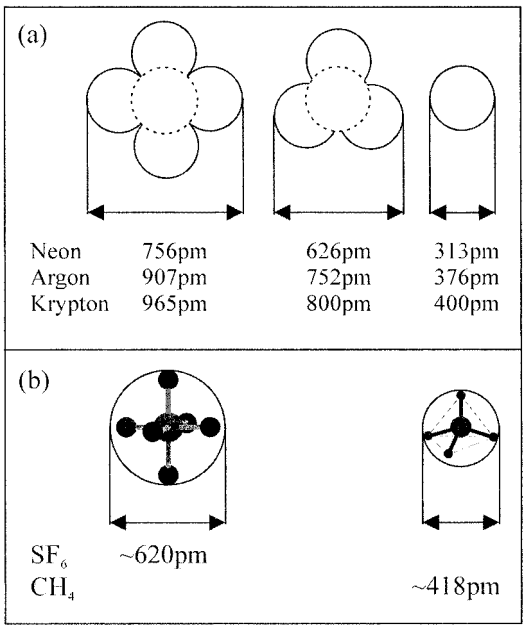

Figure 1. Schematic representation of the space requirements of monomer SF_6 and CH_4 molecules (b), confronted with likely cages in neon, argon, and krypton matrix (a).

sample is deposited onto a highly reflecting gold-plated copper (IR) or aluminum (XRD) mirror acting as sample support. The mirror was mounted at the cold end of a commercially available closed cycle He cryostat for matrix isolation studies (model Cooltower 6.5 for IR experiments and RGD 210 for XRD experiments; Leybold, Köln, Germany). The temperature of the sample support was measured with two Si diodes for the IR and an iron-doped gold/chromel thermocouple for the XRD equipment.

Neon, argon, and krypton were selected as cryogenic matrixes in order to be able to trace trends related to a well-defined scale of cage size and electron density of matrix materials. They exhibit the same solid equilibrium structures (fcc and hcp, with the transition temperatures of Ar and Kr at 60 and 80 K, respectively).[10] The deposition conditions for pure and doped matrixes were chosen such that diffusion of matrix atoms or dopant molecules is mainly avoided, which is fulfilled if the deposition temperature is below the diffusion temperature[10] of the matrix material. This is most efficiently achieved at 6.5, 14, and 20 K as the deposition temperature of Ne, Ar, and Kr, respectively, whereas the optimum deposition rate turned out to be uniformly 6 μmol min^{-1}. For a total amount of deposited sample of about 650 μmol the deposition time is then 1.5 h. All gas phase deposited samples were subjected to thermal treatment in order to investigate the influence of temperature effects such as diffusion or sintering. The maximum temperature applied in annealing experiments should, however, not exceed 12 K for Ne, 39 K for Ar, and 54 K for Kr if significant desorption of the matrix is to be avoided.

There have been extensive IR spectroscopic studies on CH_4[11−13] and SF_6[14,15] embedded in rare gas environments in the past. Therefore, our interest was focused on these molecules as probes of rare gas matrix sites. δ_{as}(C−H) (1306.2 cm^{-1} in the gas phase) and ν_{as}(S−F) (948 cm^{-1} in the gas phase) were used as test bands for CH_4 and SF_6, respectively. They exhibit reasonable values of the absorbance coefficient and react sensitively on changes in the immediate matrix environment. In Figure 1 relevant highly symmetrical substitutional sites in solid Ne, Ar, and Kr are compared to the spatial requirements of CH_4 and SF_6. Of course, the model of hard spheres applied in these estimations is a gross oversimplification. It helps, however, to exclude absolutely nonrelevant configurations.

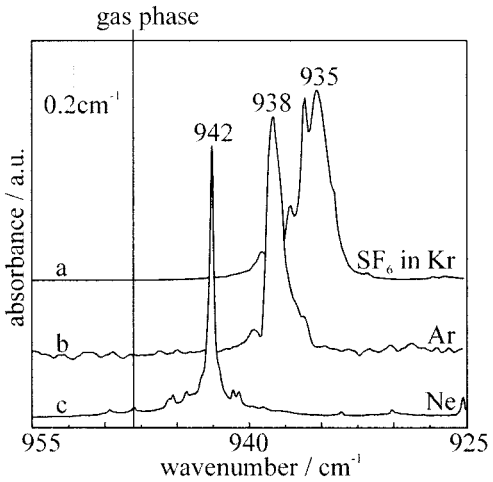

Figure 2. Comparison of the IR test band of SF_6 (ν_{as}(S−F)) after perfect isolation in Ne, Ar, and Kr (A/M = 1:1000, no annealing).

Chemicals were provided by Messer Griesheim and Linde. They were used without further purification (4.6 Ne, 6.0 Ar, 4.5 Kr, 5.0 CH_4, and 3.0 SF_6). Standard manometric procedures allowed us to quantitate the amounts of gas to be deposited as well as the concentration of mixtures (dopant/nobel gas).

Instrumentation. The IR spectra were recorded with a Fourier transform infrared spectrometer (IFS 113v, Bruker Analytische Messtechnik GmbH, Karlsruhe, Germany) equipped with a liquid nitrogen cooled MCT detector. A reflectance unit mounted in the sample compartment of the spectrometer is used to guide the beam of the light source out of the spectrometer to the cold sample support in the cryostat. Details of the whole experimental setup are described elsewhere.[16]

The X-ray diffraction patterns were recorded in a Bragg−Brentano diffractometer (Cu Kα radiation, Θ−Θ reflection geometry; Seifert, Ahrensburg, Germany) equipped with a monochromator in the primary beam. The sample is sprayed onto a gold-plated aluminum mirror on the coldfinger of the closed cycle helium refrigeration system for measurements at temperatures as low as 14 K. Its vacuum shroud contains a Mylar window that is transparent for X-rays. Data are recorded with a scintillation counter (Seifert RAE1). Details of the experimental setup are given elsewhere.[17]

Results and Discussion

The IR test band of SF_6 (ν_{as}(S−F)) in the rare gas matrixes of Kr, Ar, and Ne reveals two relevant observations (Figure 2): (1) in comparison to the gas phase, the solid rare gas environment generally shifts the band to smaller wavenumbers—the more, the higher is the atomic number of the rare gas; (2) the bandwidth as well as the complexity of the band contour increases from Ne to Ar and then to Kr.

Figure 1 demonstrates that the smallest possible cage in each of the three matrixes should be a tetrahedral 4-fold or an octahedral 6-fold substitutional site. There are two arguments that generally favor the 6-fold substitutional site: (1) the octahedral symmetry of SF_6 and (2) the monotonic trend in both bandwidth and band position of ν_{as}(S−F) with increasing atomic number of the rare gas (Figure 2). Under this assumption the isolated SF_6 molecule should preferentially probe the attractive contribution of the intermolecular interaction with the matrix cage (Ne, Ar, or Kr), and not the repulsive one. Attraction means

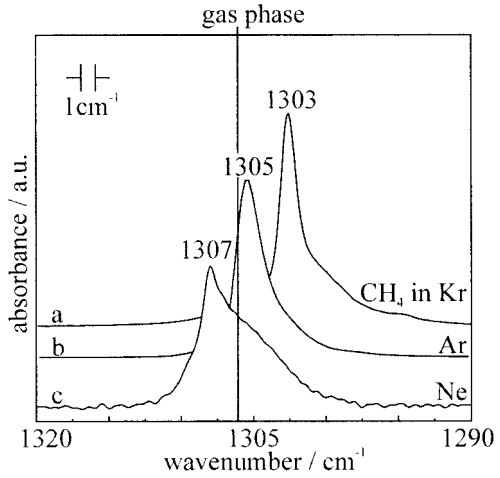

Figure 3. Comparison of the IR test band of CH_4 (ν_{as}(C−H)) after perfect isolation in Ne, Ar, and Kr (A/M = 1:1000, no annealing).

that a loss of electron density occurs in the chemical bonds of the dopant, which is reflected by a reduction of the intramolecular force field and thus of the frequencies of the respective normal vibrations. Of course, the van der Waals interactions are stronger for electron richer matrix atoms. Thus the order of the test band positions from high wavenumbers in Ne to smaller wavenumbers in Kr may intuitively be understood (Figure 2). It has, however, to be emphasized here that this assignment is not free from a certain degree of speculation. On the other hand it is, to the best of our knowledge, not in conflict with data and interpretations previously presented in the literature. The other important aspect is that, given the cage geometry, the cage size also increases in the order from Ne to Kr and not only the polarizability of the matrix material. This gives rise to an increased mobility of SF_6 in terms of librations that couple with the intramolecular mode ν_{as}(S−F). Accordingly, both the bandwidth and the complexity of the band contour augment from Ne to Ar and Kr matrix (Figure 2).

The situation for CH_4 in the three rare gas matrixes is completely different (Figure 3) from that for SF_6 (Figure 2). In Ne matrix the test band (δ_{as}(C−H)) is shifted to higher frequencies as compared to the gas phase (1306.2 cm^{-1}), indicating that the isolated CH_4 molecule being subjected to a very tight cage is squeezed by the surrounding Ne atoms, which thus positively contribute to the respective force constant. In Ar and Kr matrixes the test band goes down in frequency as compared to the gas phase value (Figure 3). This may be interpreted in terms of larger cages which, as above (SF_6), should favor the attractive influence on the intramolecular force field of CH_4 as compared to the repulsive one. On the basis of the geometrical data in Figure 1, it is difficult to imagine a squeezing effect on CH_4 in Ne in terms of anything different from a single substitutional site. Even though the corresponding site in Ar and, still more so, in Kr is significantly larger (Figure 1), a dominating effect of attraction on CH_4 appears to be doubtful in view of the spatial requirements derived from Figure 1. It has, however, to be adopted as a matter of fact: the test band in both the Ar and Kr matrix is located at smaller wavenumbers than in the gas phase. This observation is in perfect agreement with high-resolution IR studies evidencing quantized rotations of CH_4 in both Ar[18] and Kr[19] matrixes. They are certainly not in conflict with the assumption of a seemingly tight matrix cage: free rotation of an isolated molecule in condensed matter does not necessarily require a zero cage potential but rather an isotropic one. The highly symmetric single substitutional site in an Ar or Kr equilibrium solid certainly meets with this requirement reasonably well.

The IR studies discussed so far were carried out at reduced spectral resolution (0.2 cm^{-1} for SF_6 and 1 cm^{-1} for CH_4). The rotational fine structure of CH_4 in Ar and Kr[11] is not verified in the spectra of Figure 3 under these conditions. The respective test band exhibits, however, a shoulder on its low frequency wing that varies its intensity reversibly on temperature cycling the matrix sample. This is in agreement with corresponding observations in high resolution studies that unambiguously evidenced quantized rotation.[11,18,19] On the other hand, a similar shoulder related to CH_4 in Ne is more likely to be attributed to cluster formation. Temperature cycling in the small temperature interval available ($\Delta T = 5$ K) initiates only irreversible intensity changes, if any. And these changes are qualitatively identical to those observed on raising the rate or the temperature of deposition.

In a previous high resolution IR study on highly diluted SF_6 in Ar (0.01 mol %) a site specific fine structure of the test band was observed.[1,14] On temperature cycling the sample, no reversible spectral changes occurred. The irreversible ones have to be attributed to relaxation processes, eliminating local matrix structures related to sufficiently shallow potential minima. At least seven fine structure bands remain in the spectral interval between 939 and 936 cm^{-1} in the equilibrium solid after extensive annealing.[1,14] They are mainly due to different sites within the Ar cage.[14] The fascinating point is that already at a concentration as low as 0.1 mol % SF_6 in Ar the fine structure has essentially vanished. This has previously been interpreted in terms of "electromagnetically" mediated resonance broadening.[14] An inhomogeneous broadening mechanism based on SF_6−SF_6 interactions mediated "mechanically" by the Ar host, has also been proposed.[1] According to it, a distance of 10 Ar diameters or less between the next nearest SF_6 molecules no longer allows for the formation of the specific cage structures of stable SF_6 sites observed at 0.01 mol % SF_6 in Ar.[1,14] This means that each SF_6 molecule is surrounded by a structurally perturbed Ar environment that extends on the average over a distance of about five Ar diameters in each direction. The degree of structural perturbation induced by the SF_6 dopant could not be observed by X-ray diffraction via a corresponding loss of coherent X-ray scattering. The respective effect of broadening of the Bragg reflections is negligibly small as compared to that originating from the small crystallite size (<50 nm, see below). Insofar, there is presently no way of differentiating between the two broadening mechanisms observed in the IR spectrum.

In fact, already a pure Ar matrix prepared at properly selected conditions (with a deposition temperature of 14 K and a deposition rate of 6 μmol/min) exhibits the presence of two phases in the X-ray diffractogram: the crystalline fcc Ar represented by the (111) Bragg reflection and an amorphous phase giving rise to the diffuse intensity superimposed on the above-mentioned Bragg reflection (Figure 4). The crystalline fcc Ar is represented by the (111) Bragg reflection at 28.8°. Its half-width permits us to calculate the mean crystallite diameter amounting to 40−50 nm according to the Scherrer formula. This value is essentially the same for pure and for SF_6-doped solid Ar (<0.1 mol % SF_6), indicating that the influence of the SF_6-induced distortions on the half-width of the Ar Bragg reflections are negligibly small under the given experimental conditions (see above). The Bragg peak is superimposed by diffuse intensity attributed previously to a nonequilibrium Ar phase that is most likely localized close to the grain boundaries.[17] Under dynamic vacuum conditions generally applied in matrix isolation spec-

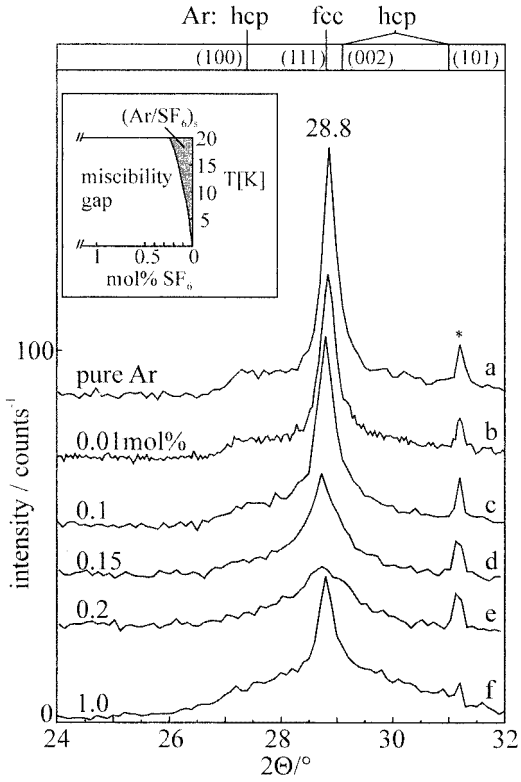

Figure 4. Diffractograms of pure solid Ar and of SF_6-doped Ar at various concentrations. The dramatic loss of coherent scattering in the small concentration interval between 0.1 and 0.2 mol % and the reappearance of partial crystallinity around 1 mol % indicate the occurrence of phase separation. This is qualitatively demonstrated by the phase diagram in the inset. For comparison, the calculated Bragg pattern of pure crystalline Ar[23] is presented as a bar diagram on top. The asterisk indicates a Bragg reflection of the sample support.

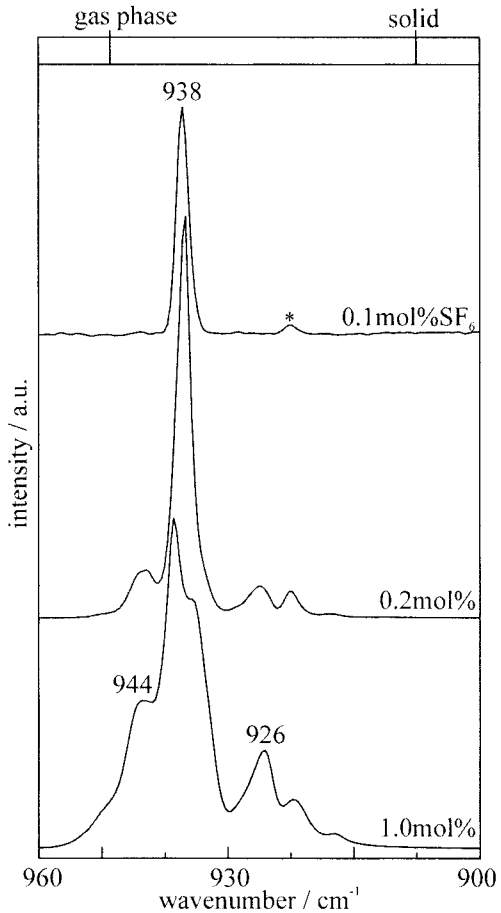

Figure 5. 5. Dimer formation manifested in the IR spectrum of SF_6 suspended in Ar matrix in the concentration interval between 0.1 and 1.0 mol % SF_6. The characteristic bands are those at 944 and 926 cm^{-1}. Relevant dimer formation is already recognizable at 0.2 mol % SF_6.

troscopy, deposition-induced morphological and structural disorder may only be reduced to a limited extent by annealing.[20] This follows from a slight decrease of the half-width of the Bragg reflection, indicating a very limited crystallite growth during the annealing procedure. In the concentration range between 0 and 0.1 mol % SF_6 (Figure 4a−c) the XRD pattern is essentially independent of the SF_6 content. Then on further raising the SF_6 concentration, dramatic changes occur (Figure 4d,e) in an extremely small interval (0.1−0.2 mol % SF_6). Around 0.2 mol % crystallinity appears to be completely lost. Later on, at 1 mol % a certain amount of crystalline phase is regained: A Bragg peak exhibiting the same position and half-width as that observed at 0.1 mol % is recovered. It is, however, superimposed by a much more abundant amorphous phase. These observations have to be interpreted in terms of a beginning phase separation. To the best of our knowledge, phase diagrams for the system Ar/SF_6 do not exist yet. Figure 4 suggests, however, that at 14 K the miscibility gap extends from the SF_6 rich phase (so far unspecified) to the concentration of about 0.1 mol % SF_6 in Ar (inset in Figure 4). The SF_6 rich phase itself does not at all contribute to the XRD pattern. Its absence may convincingly be explained by IR spectroscopic detection of SF_6 dimers, trimers, etc. at 0.1−0.2 mol % SF_6 (Figure 5). The dimer absorptions in Ar at 944 and 926 cm^{-1} have previously been assigned by Scoles et al.[21] These small aggregated species certainly do not contribute to coherent X-ray scattering and are, therefore, not seen in the XRD Bragg pattern. On the other hand, their formation necessarily implies the presence of two different Ar regions, coherently scattering ones that are free from SF_6 impurities or contain isolated monomer molecules and incoherently scattering ones that are strongly perturbed by SF_6 dimers. This is clearly visualized by the lowest trace in Figure 4. It is interesting to note that the first signs of cluster formation in the IR spectra (Figure 5) occur at concentrations for which the average distance between next nearest isolated SF_6 molecules is so small that their distorted matrix environments (five Ar atoms in each direction) start to overlap.[1] The phase separation at 14 K is certainly kinetically hindered. With increasing SF_6 concentration, increasing amounts of thermal energy are, however, introduced into the matrix via the rotational and vibrational degrees of freedom of the impurity molecule. Thus kinetic hindrance is likely to become less effective with increasing SF_6 concentration.

As mentioned previously the phase diagram for the Ar/CH_4 system is known.[3] The miscibility gap is significantly smaller than that of Ar/SF_6 (inset in Figure 4) and extends at 14 K to 2−3 mol % CH_4 (inset in Figure 6). Around this concentration two shoulders appear closely spaced to the position of the IR test band of CH_4 at 1306 cm^{-1} (Figure 7). They gain intensity on further increasing the CH_4 concentration. Therefore, they are likely to originate from dimers.

Despite the experimental evidence for phase separation and dimer/cluster formation in solid Ar/CH_4 mixtures with more than 2 mol % CH_4 at 14 K, none of the dramatic phenomena occur that were observed in Ar/SF_6 under corresponding circumstances (compare Figures 4 and 6 as well as Figures 5 and 7). Even at 10 mol % CH_4 in Ar the matrix clearly exhibits crystallinity

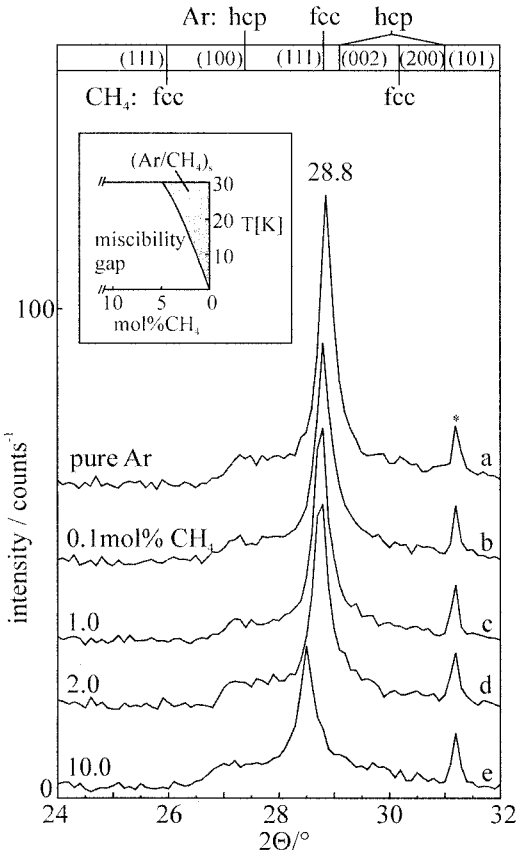

Figure 6. Diffractograms of pure solid Ar and of CH_4-doped Ar at various concentrations. There is no sudden change in the position and in the contour of the relevant Bragg peak in the concentration interval where phase separation occurs (see inset[3]). For comparison the calculated Bragg pattern of pure crystalline Ar[23] is presented as a bar diagram on top. The asterisk indicates a Bragg reflection of the sample support.

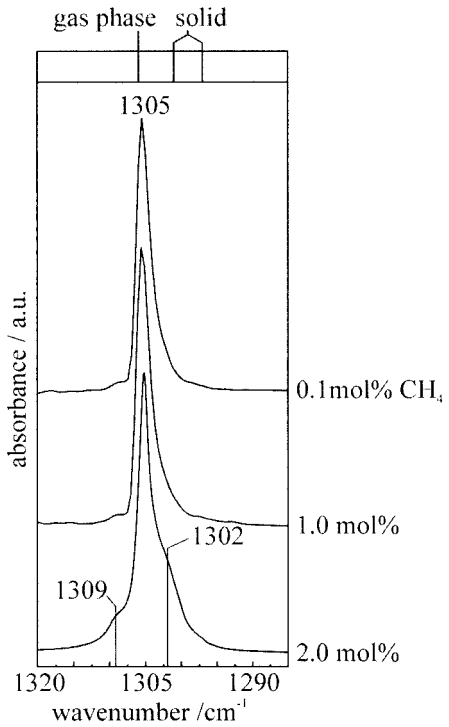

Figure 7. IR spectra of CH_4 suspended in an Ar matrix in the concentration interval between 0.1 and 2.0 mol %. First traces of dimers are recognizable at 2 mol % CH_4 via the two shoulders at 1309 and 1302 cm^{-1}.

via the fcc (111) Bragg reflection of Ar. It is, however, shifted from $2\Theta = 28.9°$ to 28.5°. This may be explained in terms of the slightly larger space requirement of a CH_4 molecule in comparison to an Ar atom (Figure 1). It contributes to an increased average lattice constant of the doped matrix. On the other hand, at 2 mol % CH_4 both position and half-width of the Bragg reflection in question are essentially equal to the respective values of pure Ar deposited under the same experimental conditions. Obviously, the lattice distortions induced by CH_4 monomers do not have any significant influence on crystallinity and on the lattice constant.

Conclusion

The present XRD studies have considerably contributed to our understanding of structure and morphology of pure and doped solid rare gas matrixes (Ar, Kr) under dynamic vacuum conditions. Both isolated CH_4 and SF_6 molecules suspended in the matrix do not significantly increase the width of the respective Bragg reflections obtained immediately after the deposition under the routine experimental conditions of high vacuum. Obviously, the dominating effect on the line width of the Bragg reflections comes from the Ar crystallite size (40−50 nm) and not from Ar lattice distortions induced by embedded isolated CH_4 or SF_6 molecules. Annealing of the matrix in the temperature regime prescribed by the high vacuum conditions does not provide any significant reduction of the Bragg reflection half width. The question arises how relevant changes in the IR spectra of matrix-isolated molecules should then be interpreted. Without any doubt they are not related to diffusion phenomena of matrix or dopant species,[22] but rather to local reorientations and rearrangements. Diffusion would favor sintering processes related to an increase of the crystallite size.

On the other hand, relevant influence of the dopant on the long-range order of the solid matrix is observed in the concentration range where dopant clustering occurs. With regard to the cluster size that initiates perturbation of the rare gas long-range order, the two molecular probes presented in this paper, CH_4 and SF_6, exhibit fundamental differences. They may be considered to represent two typical classes of molecular probes for cages in the cryogenic matrixes Ar and Kr.

The CH_4 monomer requires roughly the space of a single substitutional site in the matrix, giving rise to a minimum of dead volume. Therefore, the space required by a CH_4 dimer is then essentially the same as that for two isolated monomers. Consequently, the isolated CH_4 monomer and the two monomer units of the isolated CH_4 dimer interact with very similar matrix cages. The only difference is related to the fact that the two monomer units in the dimer are surrounded by only 11 rare gas atoms, the 12th being replaced by a methane molecule. Accordingly, there is no abrupt change in the diffraction pattern (Figure 6b−d) when the CH_4 concentration (2 mol %) allows dimer formation (Figure 7c, shoulders at 1309 and 1302 cm^{-1}). Even considerably higher CH_4 concentrations (10 mol %, Figure 6e) that should already allow the formation of a whole cluster size distribution do not destroy the crystalline structure of Ar. They do, however, clearly shift the fcc (111) Bragg peak to smaller angles. This may consistently be interpreted in terms of the slightly larger space requirement of CH_4 as compared to Ar and Kr.

The SF_6 monomer requires the space of a multiple substitutional site in the rare gas matrix, giving rise to a, in general, nonnegligible amount of dead volume. Therefore, the space required by a SF_6 dimer is then necessarily different from that

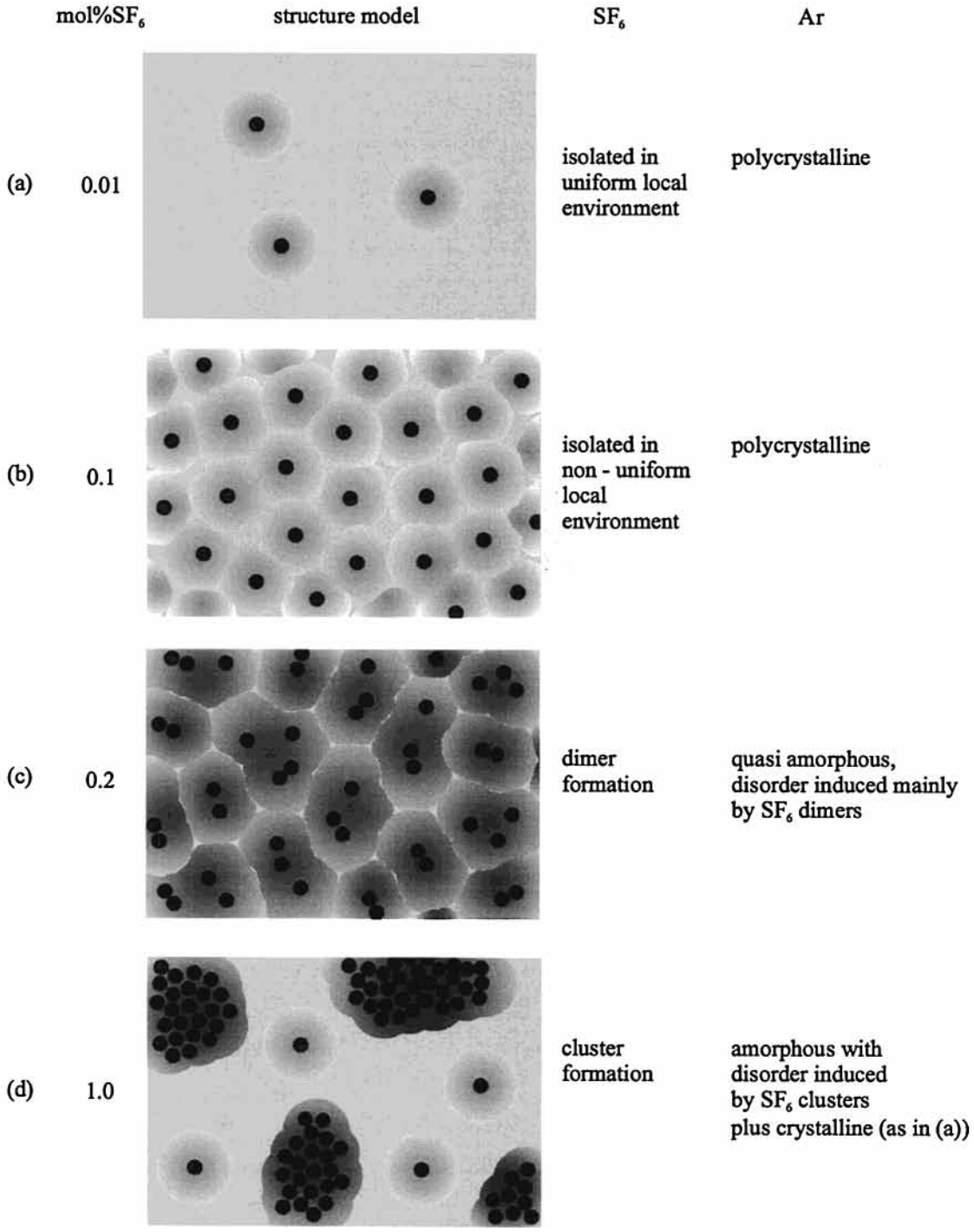

Figure 8. Schematic representation of the interplay between dimer and cluster formation of SF_6 on one hand and the degree of long-range order in the Ar matrix on the other. The intensity scale from light to dark gray represents the increasing degree of disorder (lattice distortions) in the matrix environment of SF_6 species (monomer, dimer etc.). (a), (b) Moderate lattice distortions are created by embedding SF_6 monomers in the Ar matrix (the perturbed Ar environment on the average extends over 5 Ar shells [1]). (c), (d) Strong distortions, even amorphous structures are, however, observed in the environment of SF_6 dimers and larger clusters.

of twice the multiple substitutional site for a monomer. Consequently, the isolated monomer (Figure 8a and b) and the monomer units in the dimer (Figure 8c) interact with substantially different matrix environments. As shown in Figure 4e (versus Figure 4b) the long-range order in Ar is dramatically reduced by the presence of a sufficient amount of dimers (Figure 5). At the onset of phase separation SF_6 rich matrix domains appear that contain larger but still incoherently scattering SF_6 clusters surrounded by an amorphous Ar environment (Figure 8d). At the same time SF_6 free and SF_6 monomer containing Ar domains are present.

The interesting point is that unexpected matrix effects as those described here for SF_6 may occur in the concentration range 0.1−1.0 mol %, which is extremely relevant for matrix isolation spectroscopy. They appear to be particularly likely when molecular species are to be isolated on multiple substitutional matrix sites.

Acknowledgment. Considerable financial support from the Fonds zur Förderung der Wissenschaftlichen Forschung (FWF Contract N° P11462-CHE) is gratefully acknowledged.

References and Notes

(1) Hallamasek, D.; Babka, E.; Knözinger, E. *J. Mol. Struct.* **1997**, *408/409*, 125.

(2) Greer, S. C.; Meyer, L.; Barratt, C. S. *J. Chem. Phys.* **1969**, *50*, 4299.

(3) Prager, M.; Asmussen, B.; Press, W. *J. Chem. Phys.* **1991**, *95*, 569.

(4) Grondey, S.; Prager, M.; Press, W.; Heidemann, A. *J. Chem. Phys.* **1986**, *85*, 2204.

(5) Fajardo M. E.; Tam, S. *J. Chem. Phys.* **1998**, *108*, 4237.

(6) Momose, T.; Shida, T. *Bull. Soc. Jpn.* **1998**, *71*, 1.

(7) Callegari, C.; Conjusteau, A.; Reinhard, I.; Lehmann, K. K.; Scoles, G. *J. Chem. Phys.* **2000**, *113*, 10535.

(8) Hartmann, M.; Miller, R. E.; Toennies J. P.; Vilesov, A. *Phys. Rev. Lett.* **1995**, *75*, 1566.

(9) Nauta K.; Miller, R. E. *J. Chem. Phys.* **1999**, *111*, 3426.

(10) Hallam H. E. *Vibrational Spectroscopy of Trapped Species*; Wiley: New York, 1973.

(11) Jones, L. H.; Ekberg S. A.; Swanson, B. *J. Chem. Phys.* **1986**, *85*, 3203.

(12) Cabana, A.; Savitsky G. B.; Hornig, D. F. *J. Chem. Phys.* **1963**, *39*, 2942.

(13) Frayer F. J.; Ewing, G. E. *J. Chem. Phys.* **1967**, *48*, 781.

(14) Swanson, B. I.; Jones, L. H. *J. Chem. Phys.* **1981**, *74*, 3205.

(15) Jones, L. H.; Swanson, B. I. *J. Chem. Phys.* **1983**, *79*, 1516.

(16) Knözinger, E.; Hoffmann, P.; Huth, M.; Kollhoff, H.; Langel, W.; Schrems O.; Schuller W. *Mikrochim. Acta [Wien]* **1987**, *III*, 123.

(17) Langel, W.; Becker, A.; Fleger, H.-W.; Knözinger; E. *J. Mol. Struct.* **1993**, *297*, 407

(18) Asmussen, B.; Gerlach, P.; Press: W.; Prager, M.; Blank, H. *J. Chem. Phys.* **1989**, *90*, 400

(19) Prager, M.; Langel, W. *J. Chem. Phys.* **1989**, *90*, 5889

(20) Langel, W.; Schuller, W.; Knözinger, E.; Fleger, H.-W. *J. Chem. Phys.* **1988**, *89*, 1741.

(21) Gough, T. E.; Knight, D. G.; Rowntree P. A.; Scoles, G. *J. Phys. Chem.* **1986**, *90*, 4026.

(22) Beichert P.; Pfeiler D.; Knözinger E. *Ber. Bunsen-Ges. Phys. Chem.* **1995**, *99*, 1496.

(23) Klein, M. L.; Venables, J. A. *Rare Gas Solids*; Acadamic Press: London, 1976; Vol. 2, Chapter 10.